

Prediction of Small-Strain Properties of Dry Sand Using Curve Fitting and Machine Learning Models

Pramay Bhatpahri^{1,*} and Srinivasan Gopalakrishnan¹

¹Department of Aerospace Engineering, Indian Institute of Science, Bengaluru, 560012, Karnataka, India

Abstract. This study investigates the prediction of small-strain modulus and Poisson's ratio of dry sand using both curve-fitting techniques and machine learning models. The stress-strain data utilized for this work were generated through YADE DEM triaxial simulations, which were first validated against experimental data to ensure accuracy and reliability. The small-strain modulus and Poisson's ratio were modeled as functions of confining pressure and initial void ratio. Curve-fitting techniques were employed to develop constitutive models describing these relationships. Additionally, various machine learning models were used to predict the small-strain modulus and Poisson's ratio, capturing complex nonlinear dependencies. A systematic comparison of the curve-fitting and machine learning approaches was conducted to evaluate their performance in terms of accuracy and generalizability. The findings underscore the potential of machine learning to improve predictive accuracy, offering valuable insights for soil mechanics and geotechnical engineering applications.

1 Introduction

Small-strain elastic properties of granular soils, such as Young's modulus (E), shear modulus (G), and Poisson's ratio (ν), exhibit nonlinear dependence on effective confining pressure and void ratio. Hicher [1] showed experimentally that E varies nonlinearly with mean effective stress, soil density, and stress history under small strains. Similarly, Hardin and Richart [2] demonstrated through resonant column tests that elastic wave velocities, and thus soil moduli, significantly depend on void ratio and confining pressure, reinforcing the complexity beyond simple empirical correlations.

Advancements in numerical simulations, particularly the Discrete Element Method (DEM), offer detailed insights into soil behavior by explicitly modeling particle interactions. In this study, we use YADE [3], an open-source DEM framework, to perform triaxial tests under varying confining pressures and void ratios, employing the Hertz-Mindlin (HM) contact model [4, 5]. Our goal is to assess how well this contact formulation—applied to idealized spherical particles—captures the empirical trends observed in granular materials, particularly sands, with a focus on elastic moduli (E , G) and Poisson's ratio (ν). From the simulations, we extract stress-strain curves to compute these parameters and fit classical empirical models to the DEM-derived data to establish closed-form relationships. In parallel, we implement a machine learning (ML) approach based on neural networks, offering a flexible, data-driven alternative that does not rely on fixed functional forms. By comparing these methods, we assess their predictive performance providing guidance for

selecting appropriate modeling strategies in geomechanics and wave-propagation studies.

2 Numerical Simulations and Methodology

2.1 Triaxial Simulation

The Discrete Element Method (DEM) [3] simulates granular materials by tracking particle interactions governed by Newtonian mechanics. Contact forces, modeled using spring-dashpot systems, include both normal and tangential components, while external forces such as gravity are also accounted for. The DEM workflow involves particle initialization, force computation, motion updates through numerical integration, and post-processing to analyze force distributions and particle trajectories, as illustrated in Figure 1.

A total of 372 discrete element method (DEM) triaxial simulations were performed using the Hertz-Mindlin (HM) contact model [3-5]. The DEM simulations were not based on explicit scaling laws. Instead, parameters were chosen to balance computational efficiency and coverage of a wide range of porosity and confining pressures. A particle density of 3700 kg/m^3 and stiffness $E = 100 \text{ GPa}$ were selected, consistent with mineral-based granular materials (e.g., zircon, alumina, silica, quartz). Although denser than natural sands ($\sim 2650 \text{ kg/m}^3$), this choice ensured numerical stability and allowed simulations at high confining pressures (up to 80 MPa) and low porosities (< 0.40). These parameters approximate dense granular assemblies and support the study of small-strain elastic behavior across varying void ratios and confining stresses, without aiming to replicate a specific sand type. The simulations span 12 initial target porosities (ϕ_p) ranging from 0.39 to 0.44, with void ratio computed as

*e-mail: pramayb@iisc.ac.in

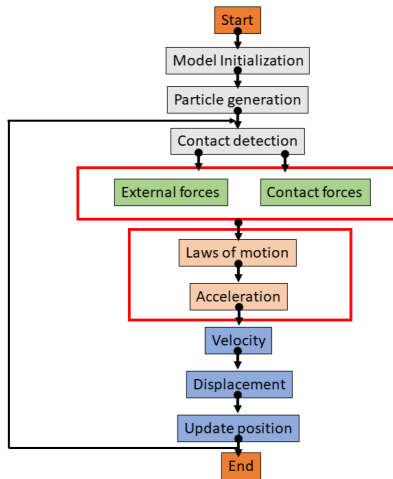


Figure 1: Typical workflow of a YADE DEM simulation.

$e = \phi_p / (1 - \phi_p)$, and 31 confining pressures (σ_{iso}) between 1 MPa and 80 MPa. The granular assembly comprises spherical particles with a mean radius of $r_m = 0.0003$ m and a relative size variability (fuzziness) of $r_{\text{fuzz}} = 0.3$, packed within a cubic domain of side length $L = 0.01$ m. Material properties assigned to the particles include a density of $\rho_{\text{particle}} = 3700$ kg/m³, Young’s modulus $E_{\text{particle}} = 100$ GPa, Poisson’s ratio $\nu_{\text{particle}} = 0.3$, and a final interparticle friction coefficient of $\mu = 0.506$. The initial packing is generated through random dense placement, followed by isotropic compression using a triaxial stress controller. Interparticle friction is dynamically reduced during compaction to promote particle rearrangement and reach the target porosity. Across all simulations, the number of particles remained nearly constant, ranging from 3872 to 3907, with a mean of approximately 3885 particles per sample. This minimal variation ($\pm 0.45\%$) ensures uniform sample size across the range of porosities and confining pressures studied. After isotropic compression, deviatoric loading is applied along the vertical axis. Key outputs such as stress–strain relationships, deviatoric stress evolution, and volumetric responses are recorded and analyzed.

2.2 Curve Fitting Methods

The small-strain moduli—Young’s modulus (E), shear modulus (G), and Poisson’s ratio (ν)—characterize the elastic behavior of granular assemblies. These were independently extracted from a carefully selected small-strain window to ensure purely elastic response. Specifically, E was obtained from the initial slope of the axial stress–strain curve, G from the shear stress–shear strain response, and ν from the ratio of lateral to axial strains. The computed values were then cross-validated using standard elastic relationships: $G = E / [2(1 + \nu)]$ and $\nu = E / (2G) - 1$, showing strong internal consistency. The average coordination number remained nearly constant within this regime, confirming that no significant microstructural changes occurred and the deformation remained elastic.

To capture the dependence of moduli on void ratio (e) and confining pressure (σ_{iso}), empirical models of the

form:

$$\text{Moduli} = f(e, \sigma_{\text{iso}}) = k \left(\frac{\sigma_{\text{iso}}}{\sigma_0} \right)^n F(e)$$

were used, where k is a material-dependent factor, σ_0 is the standard pressure, and n controls the sensitivity to confining pressure. The function $F(e)$ describes the void ratio dependence and is defined using literature-based forms:

- **Form 1** [9]: $\text{Moduli} = k \left(\frac{\sigma_{\text{iso}}}{\sigma_0} \right)^n \left(q - \frac{e^m}{1+e} \right)$
- **Form 2** [1]: $\text{Moduli} = k \left(\frac{\sigma_{\text{iso}}}{\sigma_0} \right)^n \frac{e^m}{1+e}$
- **Form 3** [2]: $\text{Moduli} = k \left(\frac{\sigma_{\text{iso}}}{\sigma_0} \right)^n \frac{(q-e)^2}{1+e}$

Here, m is an exponent determining the void ratio effect, and q is a parameter influencing the void ratio dependence. DEM simulations using the Hertz–Mindlin model provided E , G , ν , e , and σ_{iso} . Parameters were fitted using the Levenberg–Marquardt algorithm and refined with Differential Evolution to avoid local minima. Models were evaluated using the coefficient of determination (R^2) and validated against simulation data for both accuracy and physical consistency.

2.3 Machine Learning Workflow

A fully connected neural network model [6] was trained to predict Young’s modulus (E), shear modulus (G), and Poisson’s ratio (ν) from two input features: confining pressure (σ_{iso}) and void ratio (e), spanning the ranges $0.60 \leq e \leq 0.78$ and $1 \text{ MPa} \leq \sigma_{\text{iso}} \leq 80 \text{ MPa}$. The dataset was split into training (60%), validation (20%), and test (20%) subsets, and both inputs and outputs were scaled to $[0, 1]$ using Min–Max normalization. A grid search was performed over up to 39 hidden layers and 1024 neurons per layer using ReLU, Tanh, and Sigmoid activations and two optimizers (Adam, SGD). The top three architectures—ranked by validation R^2 —were retained for evaluation. To mitigate overfitting, the model incorporated dropout ($p = 0.2$) after each hidden layer, ℓ_2 weight decay (10^{-4}), and patience-based early stopping (25 epochs). Performance was assessed using 10-fold cross-validation with stratified shuffling. The mean validation score was $R^2 = 0.949 \pm 0.021$, with a training score of $R^2 = 0.955 \pm 0.006$, indicating negligible generalization gap. Although the final model contained large trainable parameters, regularization strategies ensured that its capacity remained well controlled.

3 Validation of Triaxial Code

To ensure the accuracy and reliability of our numerical simulations, we have validated our triaxial code using the Hertz–Mindlin contact model against the experimental results presented by Wu et al. (2023) [6]. Our numerical results exhibit excellent agreement with the stress–strain behavior observed in their triaxial compression experiments as illustrated in Figure 2, confirming the robustness of our implementation.

4 Results and Discussion

Three model forms are employed to estimate Young’s modulus (E) and shear modulus (G) as functions of void

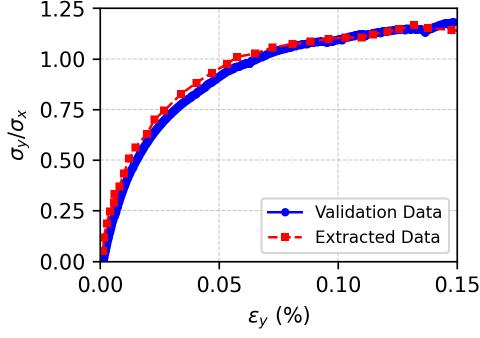


Figure 2: Validation of numerical simulation (blue circles) against the experimental results (red squares) from Wu et al. (2023) [6].

ratio and confining pressure. Each formulation incorporates a distinct combination of terms and is defined by fitted constants k , n , m , and q for both E and G . From the predicted values of E and G , Poisson’s ratio (ν) is computed using the standard elastic relation. The corresponding parameters for each model are summarized in Table 1.

Table 1: Hertz–Mindlin (HM) Model: Various Model Forms for E and G

S.N	Form	Expression	k ($\times 10^3$)	n	m	q
Young’s Modulus (E)						
1	Form 1	$E = \left[q - \frac{e^m}{1+e} \right] k \left(\frac{\sigma_{iso}}{\sigma_0} \right)^n$	5.18×10^9	0.296	5.651	0.168
2	Form 2	$E = \frac{e^m}{1+e} k \left(\frac{\sigma_{iso}}{\sigma_0} \right)^n$	1.42×10^8	0.294	-4.606	-
3	Form 3	$E = k \left(\frac{\sigma_{iso}}{\sigma_0} \right)^n \frac{(q-e)^2}{1+e}$	6.81×10^9	0.293	-	1.036
Shear Modulus (G)						
4	Form 1	$G = \left[q - \frac{e^m}{1+e} \right] k \left(\frac{\sigma_{iso}}{\sigma_0} \right)^n$	1.90×10^9	0.299	4.140	0.233
5	Form 2	$G = \frac{e^m}{1+e} k \left(\frac{\sigma_{iso}}{\sigma_0} \right)^n$	4.89×10^7	0.297	-5.049	-
6	Form 3	$G = k \left(\frac{\sigma_{iso}}{\sigma_0} \right)^n \frac{(q-e)^2}{1+e}$	3.29×10^9	0.297	-	1.007

Table 2 compares the predictive accuracy of the three forms using the coefficient of determination (R^2) for E , G , and Poisson’s ratio (ν). Form 1 shows the highest overall accuracy, followed closely by Form 3, while Form 2 performs slightly lower across all moduli. Among the three formulations, **Form 1** (see Figures 4 and 5) provides the most accurate fit across the practical range of void ratios ($0 \leq e \leq 0.8$) and confining pressures (10^5 – 10^8 Pa). Its exponential void-ratio term $\left(\frac{e^m}{1+e} \right)$ and offset parameter q enable the model to capture key trends observed in granular materials, including stiffness reduction with increasing e , a gradual nonlinear transition across intermediate confining pressures, and vanishing moduli as $\sigma_{iso} \rightarrow 0$. In contrast, **Form 2** diverges at low e due to its negative exponent, making it unsuitable for dense packings. While **Form 3** remains mathematically stable and strictly positive, it tends to overestimate stiffness at low void ratios and deviates from the simulation trends.

Table 3 summarizes the configurations and performance of neural network models used to predict E , G and ν . All models use the ReLU activation function with the

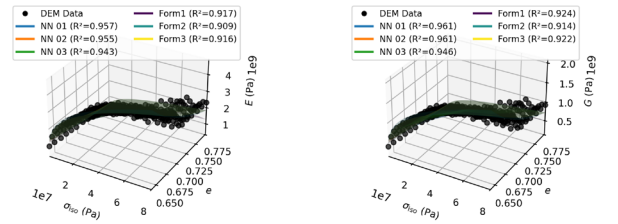
Table 2: Comparison of R^2 Scores for Different Model Forms

Form	R^2 (E)	R^2 (G)	R^2 (ν)
Form 1	0.917	0.924	0.864
Form 2	0.909	0.914	0.843
Form 3	0.916	0.922	0.804

Adam optimizer, while the number of layers and neurons per layer vary. The model with four layers and 1024 neurons achieves the highest R^2 scores across all three properties, indicating that deeper networks with higher capacity provide better predictive accuracy.

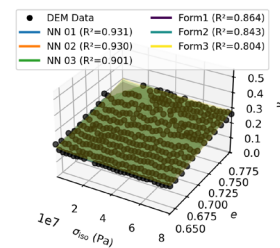
Table 3: Neural Network Model Configurations and Performance (R^2 Scores)

S.N	Layers	Neurons	Activation	Optimizer	R^2 (E)	R^2 (G)	R^2 (ν)
1	4	1024	ReLU	Adam	0.957	0.961	0.931
2	3	1024	ReLU	Adam	0.955	0.961	0.930
3	3	512	ReLU	Adam	0.943	0.946	0.901



(a) 3D plot of E vs. σ_{iso} and e .

(b) 3D plot of G vs. σ_{iso} and e .



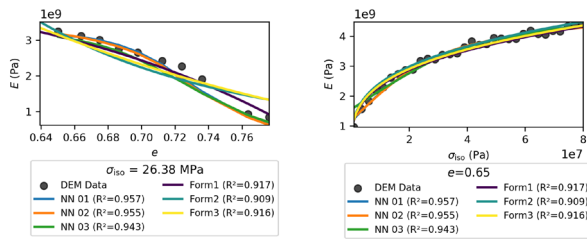
(c) 3D plot of ν vs. σ_{iso} and e .

Figure 3: 3D plots of Young’s modulus (E), Shear modulus (G), and Poisson’s ratio (ν) under varying confining pressure (σ_{iso}) and void ratio (e) for the HM (Hertz–Mindlin) Contact Model. The black dots represent the DEM data, while surfaces indicate model predictions

Figures 3–6 illustrate the variations of Young’s modulus (E), shear modulus (G), and Poisson’s ratio (ν) as functions of confining pressure (σ_{iso}) and void ratio (e). The 3D plots (Figure 3) provide an overview of these dependencies, showing that E and G increase nonlinearly with σ_{iso} while decreasing with e . In contrast, ν remains rela-

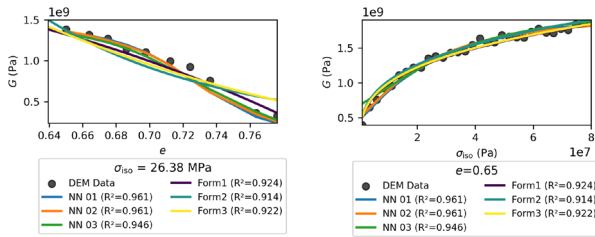
tively constant over the observed range of σ_{iso} and exhibits a slight increasing trend with e .

The 2D plots in Figures 4, 5, and 6 offer a more detailed look by isolating the effect of each variable. In particular, E and G are strongly dependent on σ_{iso} (positive correlation) and on e (negative correlation). Poisson's ratio (ν), on the other hand, remains fairly constant with changes in σ_{iso} , but shows a slight increase with e . Neural network (NN) models generally outperform empirical curve-fitting approaches in capturing these trends, although the empirical Form 1 also shows good predictive performance with interpretable parameters.



(a) E vs. e at fixed σ_{iso} . (b) E vs. σ_{iso} at fixed e .

Figure 4: 2D plots of Young's modulus (E) under varying void ratio (e) and confining pressure (σ_{iso}) for the HM (Hertz–Mindlin) Contact Model.



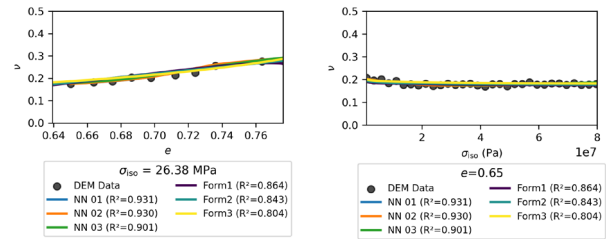
(a) G vs. e at fixed σ_{iso} . (b) G vs. σ_{iso} at fixed e .

Figure 5: 2D plots of Shear modulus (G) under varying void ratio (e) and confining pressure (σ_{iso}) for the HM (Hertz–Mindlin) Contact Model.

Overall, the NN-based approach highlights the efficacy of data-driven methods in accurately capturing the behavior of granular materials, while the empirical models remain valuable for their simplicity and interpretability, especially in scenarios where the underlying physics-based parameters are essential for practical geomechanics applications.

5 Conclusion

The discrete element method (DEM) using YADE with the Hertz–Mindlin contact model successfully captures the dependence of elastic moduli on void ratio and confining pressure in granular materials. Empirical models fit the DEM data reasonably well, with Form 1 yielding the best



(a) ν vs. e at fixed σ_{iso} . (b) ν vs. σ_{iso} at fixed e .

Figure 6: 2D plots of Poisson's ratio (ν) under varying void ratio (e) and confining pressure (σ_{iso}) for the HM (Hertz–Mindlin) Contact Model.

performance for E and G , while neural networks significantly outperform all empirical fits, especially for predicting ν . Despite these promising results, the study is limited by idealized assumptions: particles are modeled as perfect spheres without breakage or rolling resistance. These simplifications enable systematic exploration of parameter space but may overestimate stiffness at high pressures and overlook shape effects. Future work will address these limitations by incorporating rolling resistance and crushable particle models to enhance physical realism and predictive robustness.

References

- [1] Hicher, P.-Y. Elastic properties of soils. *Journal of Geotechnical Engineering*, 122(8), 641–648 (1996).
- [2] Hardin, B. O., & Richart, F. E. Jr. Elastic wave velocities in granular soils. *Journal of the Soil Mechanics and Foundations Division*, 89(1), 33–65 (1963).
- [3] Smilauer, V., Angelidakis, V., Catalano, E., Caulk, R., Chareyre, B., Chevremont, W., Dorofeenko, S., Duriez, J., Dyck, N., Elias, J., *et al.* Yade documentation. *arXiv preprint arXiv:2301.00611* (2023).
- [4] Mindlin, R. D. Compliance of elastic bodies in contact. *American Society of Mechanical Engineers*, 1949.
- [5] Mindlin, R. D. Elastic spheres in contact under varying oblique forces. *Journal of Applied Mechanics*, 16(7), 327–330 (1949).
- [6] Wu, M., Xia, Z., & Wang, J. Constitutive modelling of idealised granular materials using machine learning method. *Journal of Rock Mechanics and Geotechnical Engineering*, 15(4), 1038–1051 (2023).
- [7] Lade, P. V. *Triaxial testing of soils*. John Wiley & Sons, 2016.
- [8] Lade, P. V., & Nelson, R. B. Modelling the elastic behaviour of granular materials. *International Journal for Numerical and Analytical Methods in Geomechanics*, 11(5), 521–542 (1987).
- [9] Shibata, T., & Soelarno, D. S. Stress-strain characteristics of sands under cyclic loading. *Proceedings of the Japan Society of Civil Engineers*, 1975(239), 57–65 (1975).